

Bayesian Learning of (n,p) Reaction Cross Sections with Quantified Uncertainties

Arunabha Saha*

Department of Physics, ICFAI University Tripura, Kamalghat, Mohanpur, Tripura 799210, India

Songshaptak De

Institute of Physics, Bhubaneswar, Sachivalaya Marg, Sainik School, Bhubaneswar 751005, India

Accurate modeling of neutron-induced (n,p) reaction cross sections is essential for diverse applications in nuclear physics, including reactor design, nuclear astrophysics, and radionuclide production. However, experimental data are often sparse or incomplete, and theoretical results like TALYS Evaluated Nuclear Data Library (TENDL-2023) data may carry systematic uncertainties. In this work, we present a data-driven framework based on a Bayesian Neural Network (BNN), denoted as BNN-I6, to predict (n,p) reaction cross sections with quantified uncertainties. The model incorporates six physically motivated input features and is trained on Evaluated Nuclear Data from the ENDF/B-VIII.1 library. Leveraging stochastic variational inference, the BNN offers reliable uncertainty estimates in addition to accurate predictions. The performance of BNN-I6 is benchmarked against the TENDL-2023 library and experimental measurements across a wide range of nuclei. Additionally, SHapley Additive exPlanations (SHAP) based feature-importance analysis reveals the dominant role of theoretical cross-section inputs in driving predictions. These results highlight the potential of BNN-based approaches to enhance nuclear data evaluations and support future applications in data-scarce regimes.

I. INTRODUCTION

Nuclear reaction cross sections play a fundamental role in understanding the microscopic mechanisms governing the interaction between incident nucleons and target nuclei. Reliable knowledge of these quantities is essential for applications in nuclear astrophysics, reactor design, transmutation studies, and nuclear data evaluations. In particular, (n,p) reactions are of considerable importance because they probe charge-exchange processes that provide insights into isospin-dependent nuclear structure effects and nucleon–nucleon interactions [1, 2]. Moreover, accurate (n,p) cross sections are crucial for the production of medically important radionuclides [3]. Cross section of (n,p) reactions are also required for design calculations of nuclear reactors. In fusion reactors, bombardment of fast neutrons on the elements of first wall, structural and blanket components of the reactors leads to (n,p), (n, α), (n,n' α) and (n,n' γ) reactions. These reactions produces hydrogen and helium gases at different locations in the reactor wall. Owing to this, the mechanical properties of the reactor walls may get deteriorated. This has made the development of radiation-resistant materials for the reactors extremely important in the recent years. For this purpose, the accurate measurement of cross sections for the production of hydrogen and helium induced by neutrons with energy up to 20 MeV in the reactor materials are necessary. These cross sections are also necessary to estimate displacement per atom [4] and extent of nuclear heating.

Despite the continuous efforts in experimental nuclear physics, available cross-section data remain incomplete,

particularly for isotopes far from stability or at high incident energies. Consequently, theoretical nuclear reaction models such as those based on the Hauser–Feshbach formalism implemented in codes like TALYS-2.0 [5] and the evaluated data libraries such as TALYS Evaluated Nuclear Data Library (TENDL-2023) [6] and Evaluated Nuclear Data File (ENDF/B-VIII.1) [7] —are routinely employed to supplement missing experimental information. However, these models often depend on multiple nuclear parameters like optical model potentials, level densities, and γ -strength functions, which may introduce systematic uncertainties.

In recent years, machine learning (ML) approaches have emerged as powerful alternatives for modeling complex nonlinear relationships within nuclear data. For example, it has demonstrated tremendous success in studying heavy ion collisions [8–12], properties of strongly interacting quantum chromodynamics (QCD) matter [13–16], nuclear spallation and projectile fragmentation reactions [17–19], nuclear fission [19–23], nuclear masses [24–31], β decay half-lives and energy [32–34], α decay [35–38], charge radius of atomic nuclei [39–42], nuclear density distribution [43, 44], prediction of heavy-ion fusion cross sections [45] and evaporation residual cross sections for superheavy nuclei [46].

In comparison to the traditional machine learning methods, the Bayesian Neural Network (BNN) approach offer distinct advantage and is one of the most important approaches for studying nuclear physics because it automatically avoids overfitting and quantify uncertainties in model predictions. In recent years, significant improvements have been found using BNN on predicting nuclear mass [47], uncertainty of nuclear level density [48], quantified predictions of proton and neutron separation energies [49], nuclear charge radii [50], prediction of (n,p) reaction cross sections [51], and the drip-line

* Corresponding author; arunabhasaha@iutripura.edu.in

locations [52, 53].

The present work employs a BNN to predict the excitation functions of neutron-induced (n,p) reaction cross sections across a wide range of target nuclei. The model incorporates key nuclear parameters to learn the underlying dependencies from existing evaluated and experimental data. The predictive capability of the BNN model is systematically assessed by comparing its output with the TENDL-2023 and experimental measurements from ENDF/B-VIII.1 libraries. In addition, to gain insight into the influence of each nuclear parameter on the predicted cross sections, the SHapley Additive exPlanations (SHAP) approach [54] was utilized. This method offers a consistent and interpretable means of quantifying the importance of features in complex machine learning models. Therefore, the present study aims to establish a data-driven framework for nuclear reaction modeling, complementing conventional reaction theory approaches and contributing to the development of improved evaluated nuclear data libraries.

The rest of the paper is structured as follows. In Sec. II, we have discussed the methodology adopted in the present work, including the data preparation and BNN model implementation. In Sec. III, results are shown and discussed in detail. Finally, in Sec. IV, we have concluded our work.

II. METHODOLOGY

A Bayesian Neural Network extends the standard artificial neural network (ANN) framework by treating the network’s parameters—weights and biases—as random variables with associated probability distributions, rather than fixed values. Unlike a conventional ANN that provides a single best-fit output for a given input, a BNN yields a probability distribution over outputs. From this distribution, one can extract both a central value and credible intervals that serve as uncertainty bounds. This feature is particularly important in nuclear data modeling, where experimental measurements are often sparse and carry significant uncertainties. As a result, BNNs seem an attractive choice for modeling (n,p) reaction cross sections. A detailed exposition of the theoretical foundations and development of BNNs lies beyond the scope of this study; for a comprehensive treatment, see Refs. [55–58]. In the following subsections, we describe the dataset and the BNN model employed in our analysis.

A. Data Preparation

Our dataset consists of measured (n,p) reaction cross sections for a broad range of target nuclei (roughly $Z=8-77$) and incident neutron energies up to ~ 20 MeV. These data were drawn from evaluated nuclear data library (i.e., ENDF/B-VIII.1), ensuring a comprehensive coverage of isotopic chains and energy points.

Each data sample is described by an input–output pair $(x, \ln(\sigma_{\text{ENDF}}))$, where σ_{ENDF} is the experimentally observed cross-section (in barns) and x is a feature vector encoding the nuclear properties and reaction conditions. We design the input features to incorporate both basic nuclear properties and key physical quantities identified in previous studies [51]. In particular, each input $x = (Z, N, \delta, \Delta E, \ln(\sigma_{\text{TENDL}}), (N - Z)/A)$ includes: the proton number Z and neutron number N of the target nucleus; a pairing effect δ defined as $\delta = 1$ for even–even nuclei, 0 for odd– A nuclei, and -1 for odd–odd nuclei to capture odd–even staggering effects; the energy offset $\Delta E = E - E_{\text{thresh}}$, i.e. the incident neutron energy relative to the reaction threshold, which empirically yields more uniform excitation function patterns across isotopes; the natural logarithm of the theoretical (n,p) cross-section σ_{TENDL} ; and $(N - Z)/A$, a dimensionless measure of isospin. For incident neutron energies below 20 MeV, the cross sections of (n,p) reactions are typically less than 1 barn and can vary over several orders of magnitude. Therefore, we have used the logarithmic values of the (n,p) reaction cross sections.

For model development, a total of 8,110 data points were generated and divided into training, validation, and testing subsets. The training set (approximately 70% of the data) was used to fit the model parameters, while the validation set (comprising of 15% of the data) was employed to monitor performance and tune hyperparameters, thereby helping to prevent overfitting. The remaining 15% formed the test set, which was used to evaluate the model’s predictive capability for (n,p) cross-sections of nuclei beyond the training domain. Prior to training, we scale the proton number (Z) and neutron number (N) features by dividing them by 100 to normalize their values, which helps stabilize and speed up neural network training by keeping input features within a similar numerical range.

B. BNN Model Implementation

The BNN model is developed for a regression task aimed at predicting the experimental (n,p) cross-section from nuclear input features. The architecture comprises the following components:

- **Input layer:** Takes six input features: $(Z, N, \delta, \Delta E, \ln(\sigma_{\text{TENDL}}), (N - Z)/A)$. Note, ΔE is taken in MeV and σ_{TENDL} is in barn.
- **Hidden layers:** Two fully connected layers with 150 and 100 neurons, respectively, each employing the Exponential Linear Unit (ELU) [59] activation function to introduce nonlinearity and facilitate efficient gradient flow.
- **Output:** The model predicts two outputs for every input

- mean or central value of the target distribution (i.e., the expected cross-section).
- standard deviation σ representing the model’s inherent uncertainty in that specific prediction.

For notational purposes, we refer to our model as **BNN-I6** (a schematic diagram is shown in Fig. 1), indicating that it takes six input features.

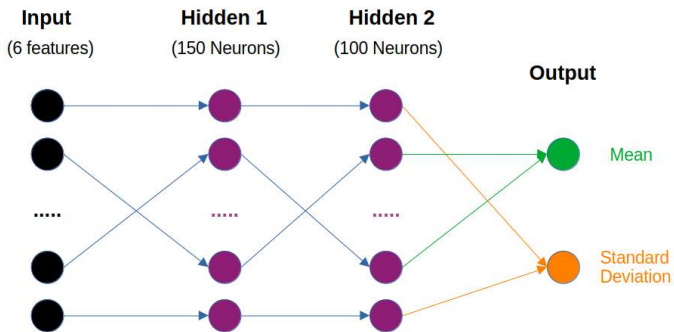


FIG. 1. (color online) A schematic diagram of our BNN-I6 model. The model consists of an input layer with six features, two hidden layers with 150 and 100 neurons respectively, and two output nodes predicting the mean and standard deviation of the target distribution.

The underlying theory of the BNN is grounded in Bayes’ theorem [60–63], which governs how prior beliefs about model parameters are updated in light of observed data. In our context, the aim is to compute the posterior distribution over the weights \mathbf{w} given the training dataset $\mathcal{D} = \{x, y\}$. This relationship is formally expressed as in Eq. 1:

$$\underbrace{P(\mathbf{w} | \mathcal{D})}_{\text{Posterior}} = \frac{\underbrace{P(\mathcal{D} | \mathbf{w})}_{\text{Likelihood}} \cdot \underbrace{P(\mathbf{w})}_{\text{Prior}}}{\underbrace{P(\mathcal{D})}_{\text{Evidence}}} \quad (1)$$

Here:

- **Prior** ($P(\mathbf{w})$): Our initial belief about the distribution of the weights before training. In our model, this is set as a simple Gaussian distribution $\mathcal{N}(0, 0.1)$ for all weights.
- **Likelihood** ($P(\mathcal{D} | \mathbf{w})$): How probable the observed data is, assuming a fixed set of weights \mathbf{w} . This is defined by the network’s output distribution, $\mathcal{N}(\mu, \sigma)$.
- **Posterior** ($P(\mathbf{w} | \mathcal{D})$): The target distribution that represents our final, learned understanding of the weights after training.

- **Evidence** ($P(\mathcal{D})$): A normalizing factor that ensures the posterior is a valid probability distribution. It is often mathematically intractable to compute for complex models like BNNs.

Because the Evidence term is often intractable in BNN, direct computation of the Posterior is not feasible. To address this, we resort to variational inference, more specifically, Stochastic Variational Inference (SVI) [64]. SVI approximates the true posterior by introducing a simpler, tractable distribution known as the variational distribution $q(\mathbf{w} | \phi)$. The parameters ϕ (comprising of means and standard deviations) are optimized to make q as close as possible to the true posterior.

The process of training a BNN involves finding the optimal distributions for all of its weights using SVI which relies on minimizing the Evidence Lower Bound (ELBO) [65, 66]. The ELBO defined in Eq. 2 serves as our loss function,

$$\mathcal{L}_{\text{ELBO}} = \mathbb{E}[\log p(y | x, \mathbf{w})] - \text{KL}(q(\mathbf{w} | \phi) \| P(\mathbf{w})) \quad (2)$$

The first term is the expected log-likelihood, which quantifies how well the model—with weights sampled from the approximate posterior $q(\mathbf{w} | \phi)$ —explains the observed data $\mathcal{D} = \{x, y\}$. Here, $p(y | x, \mathbf{w})$ represents the likelihood of the data given the weights \mathbf{w} . The model incurs a higher penalty when the true data points fall outside the predicted uncertainty range. The second term is the Kullback–Leibler (KL) divergence [67], which acts as a regularization term. It penalizes the learned weight distribution $q(\mathbf{w} | \phi)$ if it deviates significantly from the prior distribution $P(\mathbf{w})$, thereby discouraging overfitting and constraining model complexity. Thus, minimizing the ELBO is equivalent to simultaneously maximizing the data likelihood and minimizing the divergence from the prior.

Our training strategy involves two stages for effective convergence: an initial training phase of 8000 epochs with a higher learning rate ($\sim 10^{-3}$), followed by a fine-tuning phase of 1000 epochs using a reduced learning rate ($\sim 2 \times 10^{-4}$).

To quantitatively assess the model’s performance and facilitate comparison with TENDL-2023 data, we define the root mean square (r.m.s.) error metric σ_{rms} in Eq. 3:

$$\sigma_{\text{rms}} = \sqrt{\frac{1}{N} \sum_{i=1}^N (X_i^{\text{pred}} - X_i^{\text{actual}})^2} \quad (3)$$

Here, X_i^{pred} is either the BNN-I6 predicted $\ln(\sigma)$ or logarithmic value of TENDL-2023 σ data for the i -th nucleus, while X_i^{actual} denotes the $\ln(\sigma)$ value where σ is taken from ENDF/B-VIII.1 library. N represents the total number of data points used in the evaluation. In other words, σ_{rms} denotes the deviation of the BNN-I6 predicted or TENDL-2023 cross section values w.r.t. the experimental ENDF/B-VIII.1 data.

III. RESULTS AND DISCUSSIONS

In this section, we present the performance of our BNN-I6 model in predicting the experimental (n,p) cross-sections for a wide range of Z values of parent nuclei.

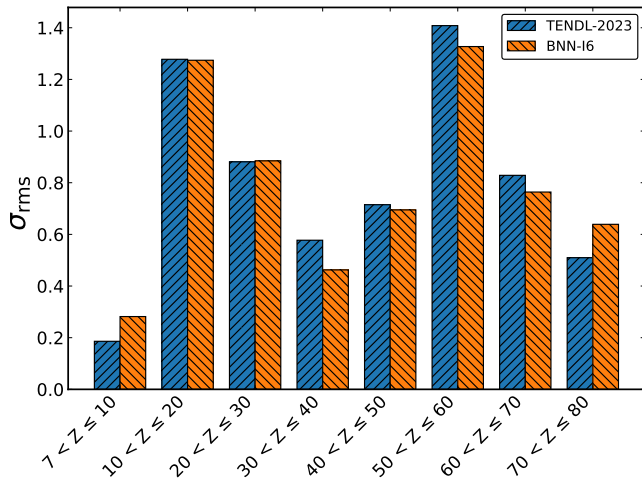


FIG. 2. (color online) σ_{rms} of (n,p) reaction cross sections predicted by the BNN-I6 model and those from the TENDL-2023 evaluation with respect to available experimental data, shown as a function of the proton-number range. The BNN-I6 predictions exhibit generally lower r.m.s. deviations across most of the nuclear landscape region. Minor fluctuations at intermediate and heavy mass ranges ($20 < Z \leq 30$) and ($50 < Z \leq 60$) reflect localized model uncertainty in those regions.

Fig. 2 presents the r.m.s. error metric (σ_{rms}) of the (n,p) reaction cross sections obtained from the BNN-I6 model and the TENDL-2023 evaluation relative to experimental data, grouped according to the proton number (Z). Overall, the BNN-based approach demonstrates strong generalization capability across the nuclear chart and effectively captures systematic reaction trends without overfitting to specific mass regions.

The subsequent discussion provides a detailed evaluation of the Bayesian neural network predictions against both the evaluated nuclear data and experimental measurements. The predictive performance of the BNN-I6 model for neutron-induced (n,p) reactions has been systematically evaluated against the TENDL-2023 library data and experimental data from the ENDF/B-VIII.1 database. The comparison is shown in Figs. 3 and 4 for representative medium- and heavy-mass nuclei, respectively. The shaded green band denote the uncertainty of the BNN predictions and the green curve denote the central line.

For the medium-mass nuclei (Fig. 3), namely ^{126}Te , ^{124}Xe , ^{160}Gd , and ^{164}Er , the BNN-I6 model reproduces the experimental excitation functions with remarkable accuracy. Across the entire incident-energy range, the BNN-I6 predictions closely match with the experimental

data, whereas TENDL-2023 shows noticeable deviations near reaction thresholds and at higher energies where the cross sections tend to saturate. The r.m.s. error metric σ_{rms} have been reported in each panel for BNN in comparison with those obtained from TENDL-2023. This improved performance arises from the Bayesian framework’s capacity to incorporate complex, nonlinear relationships between input parameters—such as proton number (Z), neutron number (N), isospin, parity etc. The uncertainty bands produced by the BNN are narrow and physically meaningful, indicating the model’s robustness.

Extending this analysis to the heavy target nuclei further elucidates the robustness of the BNN-I6 framework across a wider mass region. In the heavy target nuclei (Fig. 4), namely ^{192}Pt , ^{192}Au , ^{204}Tl , ^{207}Pb , ^{209}Bi , and ^{210}Po , the BNN-I6 model continues to demonstrate strong predictive power, despite the scarcity of experimental data in this domain. The network provides reliable estimates of the excitation functions, with uncertainty bands that encompass most of the measured data points. Notably, for ^{192}Pt , ^{192}Au , and ^{204}Tl , the BNN-I6 achieves r.m.s. deviations below 0.5. In the Pb–Bi region (^{207}Pb , ^{209}Bi , and ^{210}Po), where reaction thresholds are higher and data coverage is limited, the BNN-I6 predictions maintain reasonable agreement with the experimental data and do not exhibit overprediction.

The overall results highlight that the BNN-I6 framework successfully captures the global trends of (n,p) reaction cross sections while providing statistically meaningful uncertainty estimates. This dual capability of accuracy and uncertainty quantification makes the Bayesian neural network a promising tool for supplementing evaluated nuclear data libraries, especially in regions where experimental information is sparse or uncertain.

Building upon the observed agreement for medium- and heavy-mass systems, the subsequent analysis presents a systematic comparison of our BNN-I6 predictions with evaluated data across representative nuclei spanning the entire mass range. Fig. 5 presents a systematic comparison between the BNN-I6 predictions and the evaluated TENDL-2023 of (n,p) cross sections for representative nuclei spanning light (Na, Ca), medium-mass (Ge, Sb), and heavy (Tb, Hf) mass regions. The BNN-I6 predictions follow the global trends of the TENDL-2023 excitation functions, reproducing both the threshold behavior and the subsequent saturation pattern with increasing energy. The predictive uncertainty intervals remain narrow in the lower energy regions but gradually widen above ≈ 25 MeV, reflecting the limited availability of training data and the associated epistemic uncertainty of the model. The overall agreement between the BNN-I6 predictions and the TENDL-2023 evaluated cross sections illustrated in Fig. 5 demonstrates that the BNN framework is capable of reproducing the essential energy dependence of the (n,p) excitation functions over a wide range of target nuclei.

To provide a quantitative measure of this agreement across the nuclear chart, the r.m.s. deviations between

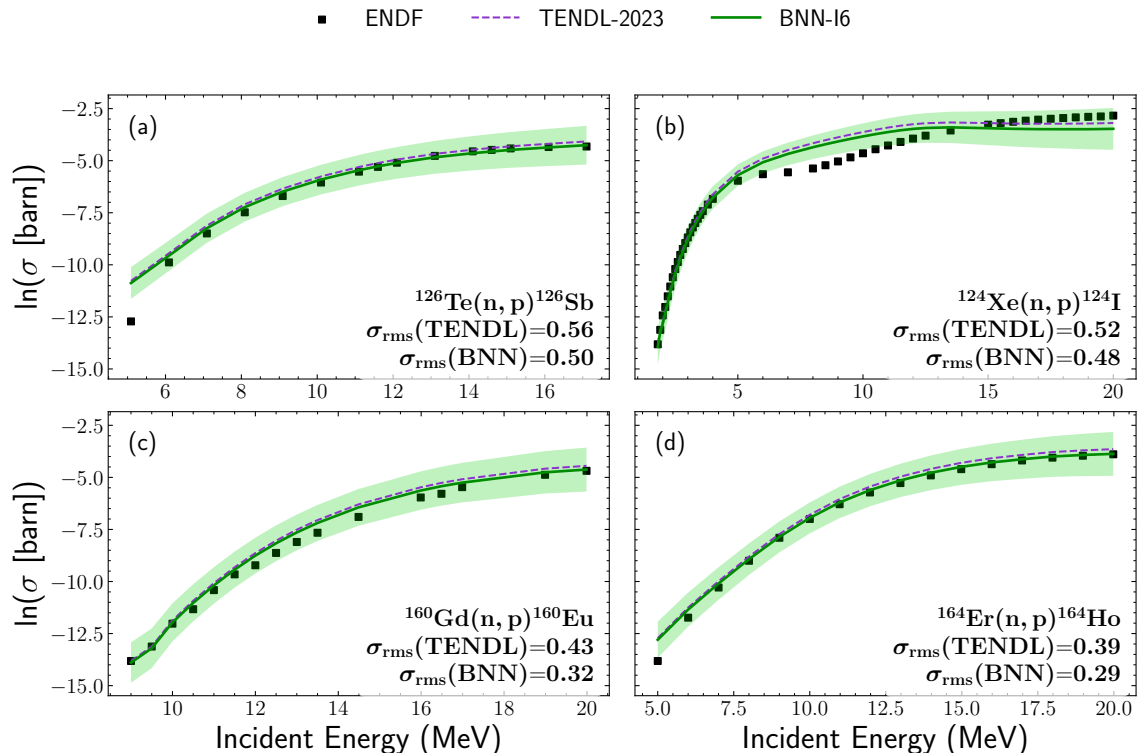


FIG. 3. (color online) Comparison of the experimental data of (n,p) reaction cross sections (solid symbols) with predictions from BNN-I6 model (solid green lines) and the TENDL-2023 data (purple dashed lines) for medium-mass target nuclei: (a) $^{126}\text{Te}(n,p)^{126}\text{Sb}$, (b) $^{124}\text{Xe}(n,p)^{124}\text{I}$, (c) $^{160}\text{Gd}(n,p)^{160}\text{Eu}$, and (d) $^{164}\text{Er}(n,p)^{164}\text{Ho}$. The shaded region denotes the uncertainty band of the BNN-predicted distributions. The corresponding r.m.s. error metric, σ_{rms} , are indicated for both TENDL-2023 and BNN-I6 in each panel. The BNN-I6 predictions follow the experimental trends closely across the full energy range, exhibiting comparable r.m.s. deviations with TENDL-2023.

the predicted and evaluated cross sections were calculated and are presented in Fig. 6. The overall distribution indicates that the majority of nuclei exhibit r.m.s. deviations below unity on the logarithmic scale, confirming the robust predictive performance of the model. The BNN-I6 model maintains a consistent level of accuracy from light to medium-mass nuclei, with modestly larger uncertainties for heavier or neutron-rich systems where experimental data are sparse and nuclear structure effects become more pronounced. This complementary analysis, thus, substantiates that the BNN-I6 model not only reproduces known reaction trends but also provides a statistically consistent quantification of predictive uncertainty across different mass regions.

Apart from what we have discussed so far, it is also necessary to understand how our BNN-I6 model works. One possible way to understand how our BNN-I6 model predicts cross sections is to find the most important features that are responsible for driving this model. SHAP is one of the most popular feature attribution methods, which we have employed in the present work to obtain the importance ranking of the input features. Fig. 7 presents a SHAP summary plot, which shows the contribution of

each input feature to the output of the trained model predicting the reaction cross section. Along the y-axis, features such as $\ln(\sigma_{\text{TENDL}})$, ΔE , δ , Z , N , and $N-Z/A$ are listed in order of their overall performance. The x-axis represents the SHAP value, indicating how strongly each feature influences the model output—positive values push the prediction higher, while negative values push it lower. The color bar represents the feature value, ranging from low (blue) to high (red). From the plot, it is evident that $\ln(\sigma_{\text{TENDL}})$ has the largest impact on the model output, showing a wide spread of SHAP values. The other features (ΔE , δ , Z , N and $N-Z/A$) have relatively minor effects, as their SHAP values are concentrated around zero. This indicates that the model prediction is primarily driven by the theoretical cross-section input, σ_{TENDL} , while nuclear and energy-related parameters play a smaller secondary role.

IV. SUMMARY

In this study, we present a Bayesian Neural Network framework, termed BNN-I6, for predicting neutron-

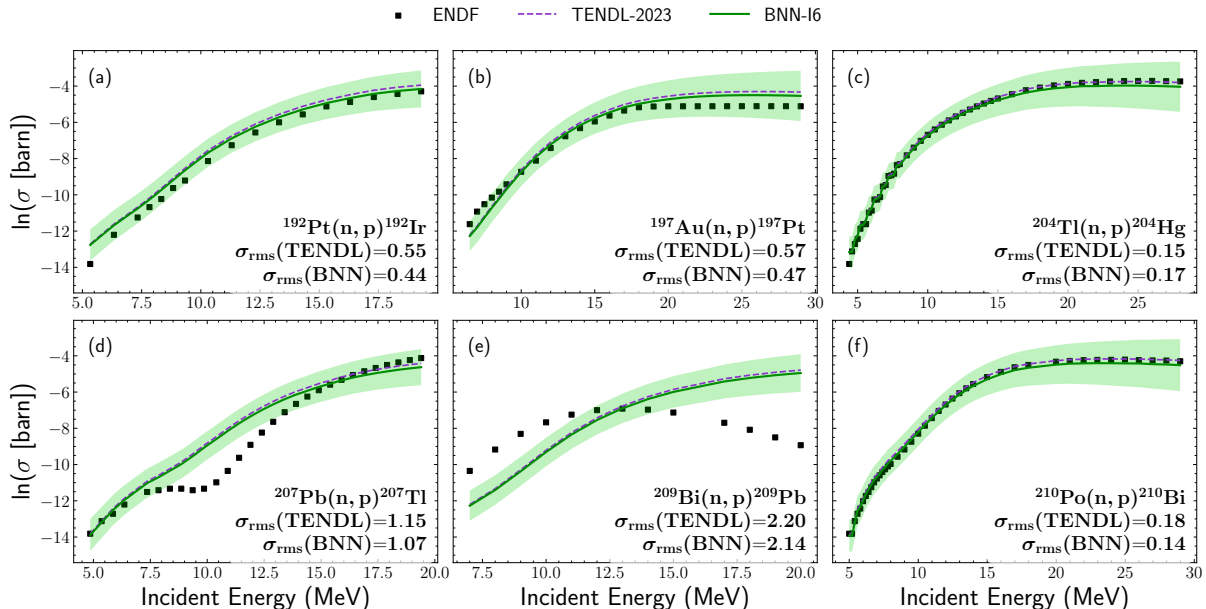


FIG. 4. (color online) Same as Fig. 2, but for heavy target nuclei: (a) $^{192}\text{Pt}(n,p)^{192}\text{Ir}$, (b) $^{197}\text{Au}(n,p)^{197}\text{Pt}$, (c) $^{204}\text{Tl}(n,p)^{204}\text{Hg}$, (d) $^{207}\text{Pb}(n,p)^{207}\text{Tl}$, (e) $^{209}\text{Bi}(n,p)^{209}\text{Pb}$, and (f) $^{210}\text{Po}(n,p)^{210}\text{Bi}$. The BNN-I6 model provides an accurate reproduction of the experimental excitation functions with narrower uncertainty bands. For nuclei in the Pb–Bi region, where reaction thresholds are high and data are sparse, the BNN-I6 model maintains reasonable agreement with the experimental data. The σ_{rms} values for BNN and TENDL are also shown for comparison.

induced (n,p) reaction cross sections across a wide range of target nuclei. The motivation stems from the critical role of accurate cross-section data in applications such as nuclear reactor design, transmutation, medical isotope production, and nuclear astrophysics, alongside the limitations of existing evaluated libraries like TENDL-2023 and the scarcity of experimental measurements for many isotopes. The BNN-I6 model uses six physically motivated input features and is trained on data from the ENDF/B-VIII.1 library. The Bayesian formalism enables the model to not only deliver accurate predictions but also quantify predictive uncertainty.

The predictive performance of BNN-I6 is systematically evaluated against both experimental data and the evaluated TENDL-2023 library data. The model shows excellent agreement with experimental excitation functions across light, medium, and heavy nuclei. Additionally, a SHAP analysis reveals that the most influential feature driving the BNN-I6 predictions is the cross-section input from TENDL-2023 library, followed by energy and nuclear structural properties.

Overall, this work demonstrates that the BNN-I6 framework provides a data-driven and uncertainty-quantified alternative to traditional nuclear reaction models. Its success in capturing complex, nonlinear dependencies makes it a promising tool for improving evaluated nuclear data libraries, especially for reactions and isotopes with limited or uncertain experimental data.

V. ACKNOWLEDGEMENTS

The author would like to acknowledge ICFAI University Tripura for all necessary helps and supports. The authors would also like to acknowledge the helpful scientific discussions and suggestions with Prof. Z. M. Niu.

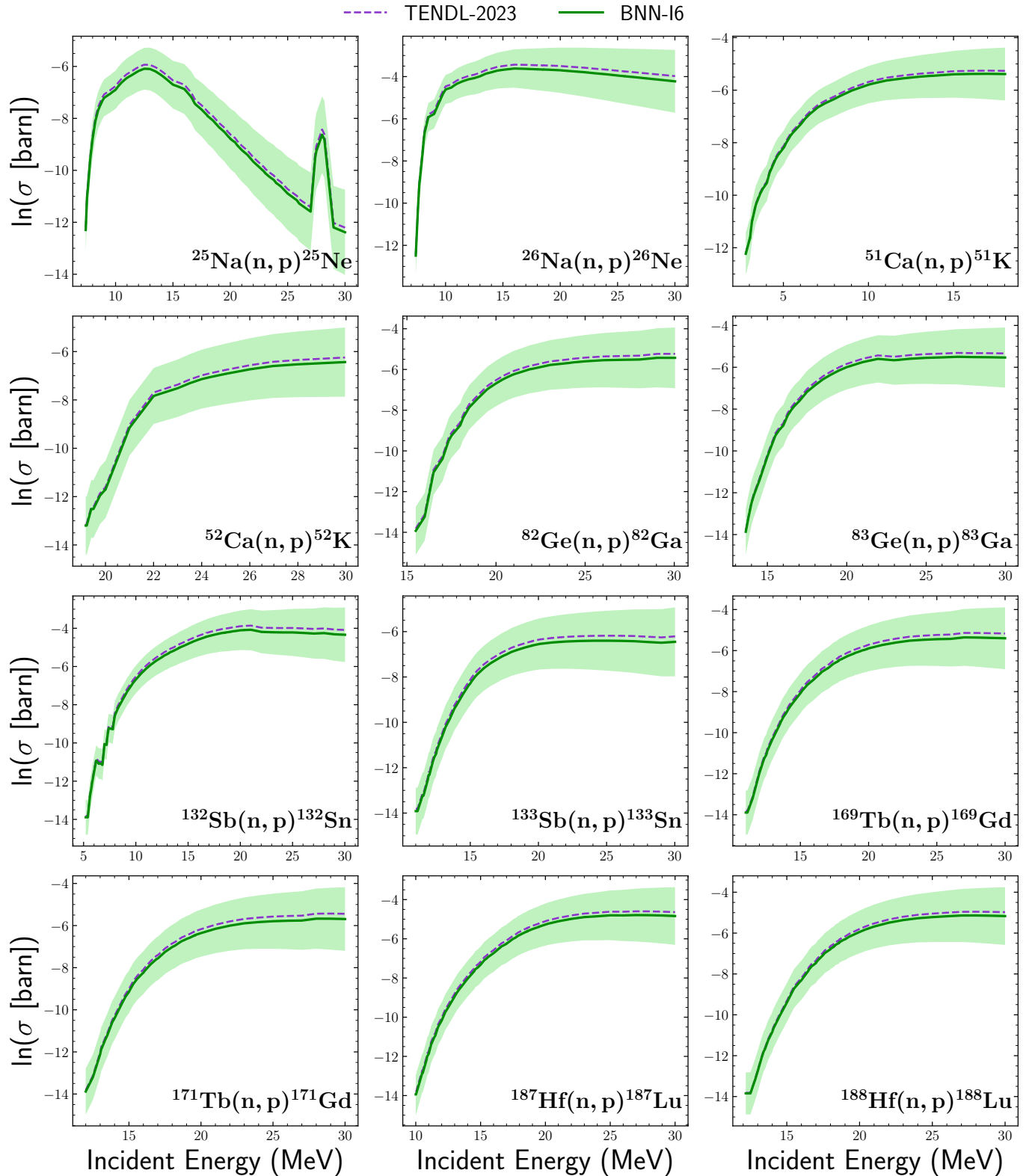


FIG. 5. (color online) Comparison of the neutron-induced (n,p) reaction cross sections obtained from the BNN-I6 model with those from the evaluated TENDL-2023 library for various target nuclei. The solid green lines represent the BNN-predicted mean values of $\ln(\sigma[\text{barn}])$, while the shaded green bands reflect the predictive uncertainty of the network. The dashed violet lines correspond to the TENDL-2023 results. The BNN-I6 model reproduces the general energy dependence of the (n,p) excitation functions and shows good agreement with TENDL-2023 predictions over most of the incident-energy range. Slight deviations and wider uncertainty intervals at higher energies primarily reflect the reduced density of training data in those regions and the increasing model uncertainty beyond the most constrained energy domain.

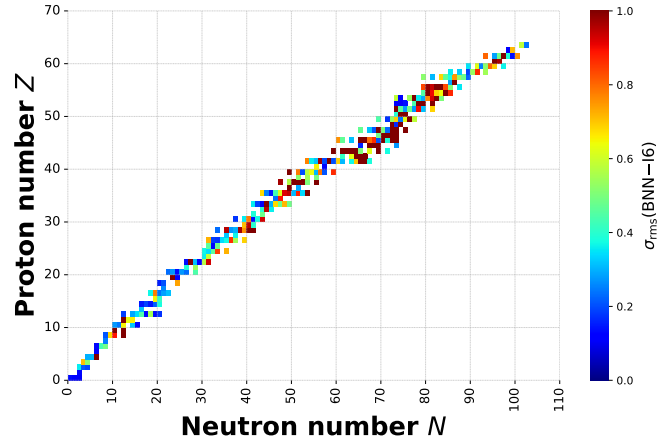


FIG. 6. (color online) R.m.s. error (σ_{rms}) between the (n,p) reaction cross sections predicted by the BNN-I6 model and the corresponding evaluated data as a function of neutron number (N) and proton number (Z). Each point represents a target nucleus, with the color scale indicating the magnitude of the r.m.s. deviation in units of $\ln(\sigma)$. The overall distribution reveals that the BNN-I6 model reproduces the evaluated cross sections with small deviations ($\sigma_{\text{rms}} < 1$) across a broad range of nuclei. Slightly enhanced deviations appear for mid-mass and heavy nuclei, which may reflect increased structural complexity and the reduced availability of experimental data in these regions. The nearly diagonal alignment of points along the line of stability demonstrates that the network effectively captures the systematic dependence of (n,p) reaction cross sections on both N and Z .

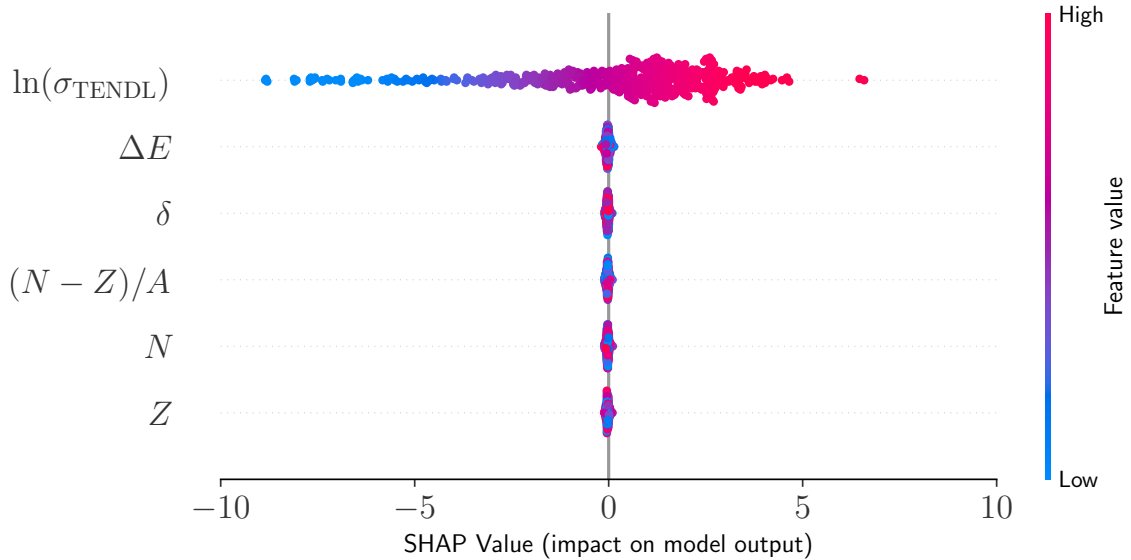


FIG. 7. (color online) Importance ranking for the input features obtained with the SHAP package. Each row represents a feature, and the x axis is the SHAP value, which shows the importance of a feature for a particular prediction. Each point represents a reaction, and the color represents the feature value (with red being high and blue being low).

-
- [1] M. Chadwick *et al.*, *Nuclear Data Sheets* **112**, 2887 (2011), special Issue on ENDF/B-VII.1 Library
- [2] C. Kalbach, *Phys. Rev. C* **33**, 818 (1986)
- [3] A. O. Jafir, H. M. Abdullah, and B. A. Gozeh, *Nuclear Engineering and Technology* **57**, 103246 (2025)
- [4] K. Kondo, S. Takagi, I. Murata, *et al.*, *Fusion Engineering and Design* **81**, 1527 (2006)
- [5] A. J. Koning, S. Hilaire, and S. Goriely, *The European Physical Journal A* **59**, 131 (2023)
- [6] A. J. Koning and D. Rochman, *Nuclear Data Sheets* **155**, 1 (2019)
- [7] D. A. Brown, M. B. Chadwick, R. Capote, A. C. Kahler, A. Trkov, M. W. Herman, A. A. Sonzogni, Y. Danon, A. D. Carlson, M. Dunn, *et al.*, *Nuclear Data Sheets* **148**, 1 (2018), eNDF database version of 2025-08-26, <https://www-nds.iaea.org/exfor/endl.htm>
- [8] Y. Wang and Q. Li, *Frontiers of Physics* **18**, 64402 (2023)
- [9] L. LI, Y. ZHANG, Y. CUI, and J. LIANG, *Sci. Sin. Phys. Mech. Astro.* **52**, 252014 (2022)
- [10] L.-G. Pang, K. Zhou, N. Su, H. Petersen, H. Stöcker, and X.-N. Wang, *Nature Commun.* **9**, 210 (2018), [arXiv:1612.04262 \[hep-ph\]](https://arxiv.org/abs/1612.04262)
- [11] W. Guojun, W. Yongjia, L. Qingfeng, and L. Fuhu, *Atomic Energy Science and Technology* **57**, 774 (2023)
- [12] Y. Wang, F. Li, Q. Li, H. Lü, and K. Zhou, *Physics Letters B* **822**, 136669 (2021)
- [13] K. Zhou, L. Wang, L.-G. Pang, and S. Shi, *Progress in Particle and Nuclear Physics* **135**, 104084 (2024)
- [14] M. O. Kuttan, K. Zhou, J. Steinheimer, A. Redelbach, and H. Stoecker, *Journal of High Energy Physics* , 184 (2021)
- [15] F.-P. Li, H.-L. Lü, L.-G. Pang, and G.-Y. Qin, *Physics Letters B* **844**, 138088 (2023)
- [16] Y.-L. Du, D. Pablos, and K. Tywoniuk, *Physical Review Letters* **128**, 012301 (2022)
- [17] D. Peng, H.-L. Wei, X.-X. Chen, X.-B. Wei, Y.-T. Wang, J. Pu, K.-X. Cheng, and C.-W. Ma, *Journal of Physics G: Nuclear and Particle Physics* **49**, 085102 (2022)
- [18] C.-W. Ma, X.-B. Wei, X.-X. Chen, D. Peng, Y.-T. Wang, J. Pu, K.-X. Cheng, Y.-F. Guo, and H.-L. Wei, *Chinese Physics C* **46**, 074104 (2022)
- [19] Q. Song, L. Zhu, B. Cai, C. Yuan, J. Su, and H. Guo, *Physical Review C* **107**, 044609 (2023)
- [20] A. E. Lovell, A. T. Mohan, and P. Talou, *Journal of Physics G: Nuclear and Particle Physics* **47**, 114001 (2020)
- [21] Z.-A. Wang, J. Pei, Y. Liu, and Y. Qiang, *Physical Review Letters* **123**, 122501 (2019)
- [22] Z.-A. Wang and J. Pei, *Physical Review C* **104**, 064608 (2021)
- [23] Z. Wang, J. Pei, Y. Chen, C. Qiao, F. Xu, Z. Ge, and N. Shu, *Physical Review C* **106**, L021304 (2022)
- [24] M. Mumpower, T. Sprouse, A. Lovell, and A. Mohan, *Physical Review C* **106**, L021301 (2022)
- [25] A. E. Lovell, A. T. Mohan, T. M. Sprouse, and M. R. Mumpower, *Physical Review C* **106**, 014305 (2022)
- [26] Z. Niu and H. Liang, *Physics Letters B* **778**, 48 (2018)
- [27] Z.-P. Gao, Y.-J. Wang, H.-L. Lü, Q.-F. Li, C.-W. Shen, and L. Liu, *Nuclear Science and Techniques* **32**, 109 (2021)
- [28] X.-C. Ming, H.-F. Zhang, R.-R. Xu, X.-D. Sun, Y. Tian, and Z.-G. Ge, *Nuclear Science and Techniques* **33**, 48 (2022)
- [29] X. Wu, L. Guo, and P. Zhao, *Physics Letters B* **819**, 136387 (2021)
- [30] T. Zhao and H. Zhang, *Nuclear Physics A* **1021**, 122420 (2022)
- [31] X.-K. Le, N. Wang, and X. Jiang, *Nuclear Physics A* **1038**, 122707 (2023)
- [32] L. Peng, B. JingHu, N. ZhongMing, and N. YiFei, *SCIENTIA SINICA Physica, Mechanica & Astronomica* **52**, 252006 (2022)
- [33] Y.-F. Gao, B.-S. Cai, and C.-X. Yuan, *Nuclear Science and Technology* **34**, 9 (2023)
- [34] J. M. Munoz, S. Akkoyun, Z. P. Reyes, and L. A. Pachon, *Physical Review C* **107**, 034308 (2023)
- [35] C.-Q. Li, C.-N. Tong, H.-J. Du, and L.-G. Pang, *Physical Review C* **105**, 064306 (2022)
- [36] N.-N. Ma, T.-L. Zhao, W.-X. Wang, and H.-F. Zhang, *Physical Review C* **107**, 014310 (2023)
- [37] Z. Yuan, D. Bai, Z. Ren, and Z. Wang, *Chinese Physics C* **46**, 024101 (2022)
- [38] Z. Jin, M. Yan, H. Zhou, A. Cheng, Z. Ren, and J. Liu, *Physical Review C* **108**, 014326 (2023)
- [39] X.-X. Dong, R. An, J.-X. Lu, and L.-S. Geng, *Physics Letters B* **838**, 137726 (2023)
- [40] P. Su, W.-B. He, and D.-Q. Fang, *Symmetry* **15**, 1040 (2023)
- [41] D. Wu, C. Bai, H. Sagawa, and H. Zhang, *Physical Review C* **102**, 054323 (2020)
- [42] X.-X. Dong, R. An, J.-X. Lu, and L.-S. Geng, *Physical Review C* **105**, 014308 (2022)
- [43] Z.-X. Yang, X.-H. Fan, P. Yin, and W. Zuo, *Physics Letters B* **823**, 136650 (2021)
- [44] T.-S. Shang, J. Li, and Z.-M. Niu, *Nuclear Science and Techniques* **33**, 153 (2022)
- [45] Z. Li, Z. Gao, L. Liu, Y. Wang, L. Zhu, and Q. Li, *Physical Review C* **109**, 024604 (2024)
- [46] T. L. Zhao, X. J. Bao, and H. F. Zhang, *Nuclear Physics A* **1027**, 122510 (2022)
- [47] R. Utama, J. Piekarewicz, and H. B. Prosper, *Physical Review C* **93**, 014311 (2016)
- [48] X. Wang, Y. Cui, Y. Tian, K. Zhao, and Y. Zhang, *Chinese Physics C* **48**, 084105 (2024)
- [49] L. Neufcourt, Y. Cao, S. A. Giuliani, W. Nazarewicz, E. Olsen, and O. B. Tarasov, *Physical Review C* **101**, 044307 (2020)
- [50] R. Utama, W.-C. Chen, and J. Piekarewicz, *Journal of Physics G* **43**, 114002 (2016)
- [51] W. F. Li, L. L. Liu, Z. M. Niu, Y. F. Niu, and X. L. Huang, *Physical Review C* **109**, 044616 (2024)
- [52] L. Neufcourt, Y. Cao, W. Nazarewicz, and F. Viens, *Physical Review C* **98**, 034318 (2018)
- [53] L. Neufcourt, Y. Cao, W. Nazarewicz, E. Olsen, and F. Viens, *Physical Review Letters* **122**, 062502 (2019)
- [54] S. M. Lundberg and S.-I. Lee, in *Proceedings of the 31st International Conference on Neural Information Processing Systems* (Curran Associates Inc., Long Beach, California, USA, 2017) pp. 4768–4777
- [55] C. M. Bishop, *Neural Networks for Pattern Recognition* (Oxford University Press, Oxford, UK, 1995)

- [56] R. M. Neal, *Bayesian Learning for Neural Networks*, Lecture Notes in Statistics, Vol. 118 (Springer, New York, 1996)
- [57] S. Haykin, *Neural Networks: A Comprehensive Foundation*, 2nd ed. (Prentice Hall, Upper Saddle River, NJ, 1999)
- [58] V. N. Vapnik, *Statistical Learning Theory* (Wiley-Interscience, New York, NY, 1998)
- [59] D.-A. Clevert, T. Unterthiner, and S. Hochreiter, *Fast and accurate deep network learning by exponential linear units (elus)* (2016), arXiv:1511.07289 [cs.LG]
- [60] J. Earman, in *Hume's Abject Failure: The Argument Against Miracles* (Oxford University Press, 2000)
- [61] S. E. Fienberg, *Bayesian Analysis* **1**, 1 (2006)
- [62] B. Efron, *Science* **340**, 1177 (2013)
- [63] D. P. Berrar, in *Encyclopedia of Bioinformatics and Computational Biology* (2019)
- [64] M. D. Hoffman, D. M. Blei, C. Wang, and J. Paisley, *Journal of Machine Learning Research* **14**, 1303 (2013)
- [65] D. M. Blei, A. Kucukelbir, and J. D. McAuliffe, *Journal of the American Statistical Association* **112**, 859 (2017), <https://doi.org/10.1080/01621459.2017.1285773>
- [66] D. P. Kingma and M. Welling, *Auto-encoding variational bayes* (2022), arXiv:1312.6114 [stat.ML]
- [67] S. Kullback and R. A. Leibler, *The Annals of Mathematical Statistics* **22**, 79 (1951)